JOURNAL OF SOLID STATE CHEMISTRY 66, 56–63 (1987)

The Effects of Cation Substitution on the Hollandite-Type Structure

MAMORU WATANABE AND YOSHINORI FUJIKI

National Institute for Research in Inorganic Materials, Namiki 1-1, Sakura-mura, Niihari-gun, Ibaraki 305, Japan

AND YASUO KANAZAWA AND KATSUHIRO TSUKIMURA

Geological Survey of Japan, Higashi 1-1-3, Yatabe, Tsukuba-gun, Ibaraki 305, Japan

Received January 17, 1986; in revised form April 15, 1986

Hollandite-type tunnel structures of $K_{1.50}Al_{1.50}Ti_{6.50}O_{16}$ and $Rb_{1.47}Al_{1.47}Ti_{6.53}O_{16}$ were refined; final *R*- and *wR*-factors were 2.24/3.30 and 2.98/3.32%, respectively. The structures were compared with those of $K_{1.54}Mg_{0.77}Ti_{7.23}O_{16}$ and $BaAl_2Ti_6O_{16}$ from the viewpoint of crystal chemistry. The substitutions of K by Rb and Ba make an anisotropic deformation on the frameworks relative to that of $K_{1.50}Al_{1.50}Ti_{6.50}O_{16}$, whereas the replacement of Al by Mg changes more uniformly the network by enlarging octahedra themselves. The octahedron in the three priderites, (Rb, K, or Ba)$_x$Al$_y$Ti$_{8-y}$O$_{16}$, becomes larger and gets more regular in that order, but the off-center displacement of the octahedral cation also becomes larger. The volume-dependent octahedron regularity is due to the sensitive movement of bottleneck oxygen atoms with the differences in charge and/or size among the tunnel ions. The volume dependency of the off-centering seems to be explicable on the basis of Megaw's theory.

Introduction

Some priderites are known as 1-D fast ion conductors for alkali ions, especially K^+, and some of them containing Cs^+ and Ba^{2+} have been studied as nuclear waste immobilizers.

The general chemical formula of priderites is $A_xB_yTi_{8-y}O_{16}$, where *A* are primarily alkali or alkaline earth ions and *B* are di- or trivalent cations. They are isostructural to the mineral "hollandite" and usually have tetragonal symmetry. The existence of 1-D large tunnels along the unique axis is a typical structural feature and these tunnels are about four times larger in area than rutile-type channel. They nonstoichiometrically accommodate the *A* ions so as to charge-neutralize the partial replacement of Ti^{4+} by the $B^{2+ \text{ or } 3+}$ in the framework.

In the hollandite-type ionic conductors, the *A* ions are regarded as mobile species. The ionic conductivities have been found to depend on temperature and frequency (1, 2) in a manner different from the thermal activation-type ion conductors. Recently, it was reported (*3*) that the highly purified priderites, $K_xAl_xTi_{8-x}O_{16}$ and $K_{2x}Mg_xTi_{8-x}O_{16}$, might have the frequency independent part of conductivity, i.e., a potentiality of dc conduction. The conductivity and activation energy estimated by the equivalent cir-

0022-4596/87 $3.00

cuit method were about 10^{-2}S/cm at 300 K and 0.28 eV, which were comparable to those of the dc-conductive Na–β–Al_2O_3. So far, conduction phenomena in a variety of priderites which contain mainly Mg^{2+} or Al^{3+} for the octahedral cation and K^+, Rb^+, and/or Cs^+ for the tunnel ion have been investigated by the ac method (*1–4*), NMR (*5*), and Raman and IR (*6, 7*), and the behaviors of the mobile ions have been explained. Those priderites were examples relevant to the 1-D conduction phenomena of ions, and a theory based on the Frenkel–Kontrova model was presented in order to explain the conduction behavior of K^+ in $K_{1.54}Mg_{0.77}Ti_{7.23}O_{16}$ (*8*).

We study in detail the structural influences of cation substitution on the hollandite-type networks and discuss the results from the viewpoint of crystal chemistry. In this paper, we are especially interested in the effects of tunnel cation substitution. In the model quoted above, a total potential of the system is assumed as the first approximation to be a sum of the framework potential and the interaction energy between mobile ions. Actually there should be an interaction between the tunnel cations and the framework ions. We extract such an interaction from the structural aspect.

The crystal structure of hollandite was first determined by Byström and Byström (*9*). Since then several reports have been published for structure refinements of natural and synthetic hollandites and priderites (*10–12*) and relatives (*13, 14*).

Priderite Structure

The priderite structure with space group *I*4/*m* is projected along [001] in Fig. 1. Its network is constructed by a simple edge-shared linkage of the rutile-type channel units (*15*) resulting in the hollandite-type and the rutile-type tunnels in equal numbers. The unit cell contains eight equivalent octahedra or $(B,Ti)_8O_{16}$ in composition. Due to partial substitution of the di- or tri-

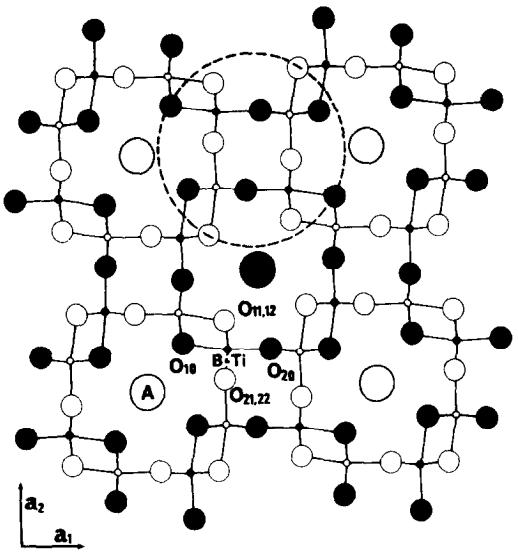

FIG. 1. [001] projection of priderite structure. The nearest neighbors of tunnel ions are all crystallographically equivalent to O_{10}, and the remaining oxygen atoms can be derived from O_{20} by the symmetry operations. The linkage of octahedra in a dotted line circle represents a rutile-type channel unit, which is the basic subunit of a priderite framework. Filled circles are located at $z = 0$ and open ones at $z = \frac{1}{2}$.

valent *B* ions for Ti^{4+}, the framework has a net negative charge. This is compensated for by the introduction of an appropriate number of type *A* cations into the larger channels; this process gives the chemical formula of $A_xB_yTi_{8-y}O_{16}$.

In the structure, the *A* ion is coordinated by eight equivalent oxygen atoms at the corners of a tetragonal prism. Basal planes of this prism are shared with the adjacent prisms in the same tunnel, and hence they are bottleneck windows into the following unit cells along the *c*-axis. The site (2a) at the center has 4/*m* point symmetry. In most priderites, some of the *A* ions are displaced from the sites along the tunnel axis because of the coulombic repulsive forces between tunnel cations. These off-centered sites keep only fourfold axial symmetry and are denoted as the (4e) sites. All atoms except for the *A* ions on these sites are located on

mirror planes normal to the c axis at $z = 0$ and $\frac{1}{2}$.

Experimental

$K_xAl_xTi_{8-x}O_{16}$ (hereafter KATO) and $Rb_xAl_xTi_{8-x}O_{16}$ (RATO) crystals were grown by the slow cooling technique (*16*) from flux melts of highly purified systems K_2CO_3–MoO_3 and Rb_2CO_3–MoO_3, respectively. The crystals were acicular with well-developed {100} and {110} faces and were yellow in color. Using a small crystal of KATO (0.3 × 0.3 × 0.7 mm), precession and Weissenberg photographs were taken to confirm the symmetry. The observed diffraction patterns indicated Laue symmetry $4/m$ and $h + k + l = 2n$ for extinction rule and were accompanied by diffuse scatterings concentrated on reciprocal lattice planes perpendicular to the unique axis (*17*). The densities of KATO and RATO were measured using about 600 mg of single crystals by the previous method (*18*). Nearly spherical crystals, which were rounded in advance and were ~240 and ~220 μm in diameter for KATO and RATO, were subjected to lattice constants and diffraction intensity measurements on a four-circle automatic diffractometer (Rigaku AFCV) using pyrolytic graphite monochromated Mo$K\bar{\alpha}$ radiation. Intensity data were measured below a 2θ of 110° in the quarter Ewald sphere by the 2θ–θ continuous scanning method with a 2θ-scan speed of 2°/min and corrected for Lp effects. As to weak reflections, intensity measurements were repeated up to 10 times at the maximum. About 1890 F_o and $\sigma(F_o)$ pairs with hkl and $\bar{h}kl$ were collected for KATO and averaged among their crystallographic equivalents, resulting in about 900 independent reflections. Omitting 25 reflections with $F_o = 0$ and 10 with $F_o < 3\sigma(F_o)$ from them, the remainders were used for the following refinement. Rato gave 1918 pairs and 950 independent reflections after averaging. Excluding $F_o = 0$ and $F_o < 3\sigma(F_o)$, 813 reflections were utilized for refinement.

Refinement

The refinements were carried out by means of the full matrix least-squares program (*19*). The function $\Sigma w(|F_o| - k|F_c|)^2$ was minimized in the program, where k is a scale factor and w the weight of $1/\sigma(F_o)^2$. Fourier and d-Fourier synthetic methods (*20*) were used along with the above. Atomic scattering factors of K^+, Rb^+, Al^{3+}, and Ti^{4+} were taken from the International Tables for X-Ray Crystallography (*21*) and that of O^{2-} from the reference (*22*). F_o values were corrected for spherical absorption effect whose factors were also quoted from the above handbook, and isotropic extinction and anomalous dispersion corrections were made. Anomalous scattering factors were given from the report (*23*).

F_o data were prescaled with the known coordinates and thermal parameters (*2*), and chemical compositions obtained from the analyses ($x \sim 1.50$ in KATO and 1.47 in RATO), where the alkali ions were kept at $z = \frac{1}{2}$ or (2a) site. After some cycles, the reliability factors of KATO and RATO data sets were ~11 and ~19%, respectively. The temperature factors of K^+ and Rb^+ were about 10 in $8\pi^2\bar{u}^2$. In this stage, Fourier maps were synthesized to look at positional distributions of these alkali ions. The K^+ showed three clear peaks located at $z_k = \frac{1}{2}$ and $\frac{1}{2} \pm 0.17$. On the other hand, the Rb^+ had a nearly flat-top peak ranging over $|z_{Rb} - \frac{1}{2}| < 0.09$ which seemed to consist of two equivalent peaks placed near $z_{Rb} = \frac{1}{2} \pm 0.09$. In the following steps of refinement, two split atom models were applied to the alkali ions, (a) the first model consisting of two (4e) sites with $z = \frac{1}{2} \pm \Delta z$ and (b) the second having $z = \frac{1}{2}$ and $\frac{1}{2} \pm \Delta z$. In addition, the best type of extinction correction was examined among four combinations of Gaussian or Lorentzian distribution of mo-

saic spread or particle size. The Lorentzian and Gaussian distributions of particle size gave the best improvements of reliability factors for either compound. The two distribution types resulted in no substantial differences in the factors. In this stage, KATO and RATO had ~5 and ~9% in R-factor under isotropic thermal parameters, respectively. The KATO data set was best-fitted with the second model, and the differences in R- and weighted $R(= wR)$-factors between the two models were only ~0.5 and ~0.2%, respectively, even when anisotropic temperature factors were introduced. The second model, however, displayed smoother residual contours on d-Fourier maps than the other. The F_o data of RATO were effectively adjusted by the first model, whereas the second led to unfavorable solutions owing to strong correlations among z_{Rb}, B_{33}, and w_{Rb} in spite of using damping factors.

Additional refinements including chemical compositions were carried out; that is, the occupancies of K^+, Rb^+, and Al^{3+} were changed as subsidiary variables of the Ti^{4+} content. The R- and wR-factors of KATO were hardly improved. On the other hand, RATO gave an improvement of 0.56% in wR, but the corresponding R-factor was kept almost the same: 2.98/3.32 → 3.02/2.76 in R/wR. In this refining, the Rb (or Al) content was reduced from 1.47 to 1.41, and only z_{Rb} and B_{Rb} varied over their standard deviations: z_{Rb}, 0.6214 → 0.6201 and B_{Rb}, 2.57 → 2.33.

TABLE I

LATTICE CONSTANTS AND DENSITIES OF KATO AND RATO

$K_{1.50}Al_{1.50}Ti_{6.50}O_{16}$	$Rb_{1.47}Al_{1.47}Ti_{6.53}O_{16}$
a = 10.062(1) Å	a = 10.110(1) Å
c = 2.9369(1) Å	c = 2.9375(1) Å
ρ_0 = 3.73(1)	ρ_0 = 4.03(1)
ρ_c = 3.720	ρ_c = 4.069

TABLE II

FINAL POSITIONAL AND THERMAL PARAMETERS

(a)

Atom	X	Y	Z	B (Å²)
K1	0	0	0.5	2.9(2)
K2	0	0	0.700(2)	2.5(2)
Ti(Al)	0.3515(1)	0.1678(1)	0	0.59(1)
O1	0.1552(1)	0.2054(1)	0	0.39(3)
O2	0.5407(1)	0.1652(1)	0	0.47(3)

Note. R = 2.24% and wR = 3.30%; $g = 1.54 \times 10^{-4}$ cm.

(b)

Atom	X	Y	Z	B (Å²)
Rb	0	0	0.6214(6)	2.57(5)
Ti(Al)	0.3507(1)	0.1669(1)	0	0.79(2)
O1	0.1562(2)	0.2073(2)	0	0.59(5)
O2	0.5398(2)	0.1655(2)	0	0.67(5)

Note. R = 2.98% and wR = 3.32%; $g = 0.86 \times 10^{-4}$ cm.

Results and Discussions

KATO and RATO lattice constants and densities are shown in Table I. Final atomic positions and thermal parameters are listed in Tables IIa and b together with final R- and wR-factors and extinction parameters in the margins.[1] B-factors in the last columns were converted from their anisotropic thermal parameters. Interatomic distances are listed with respect to $(B,Ti)O_6$ (hereafter MO_6) and AO_8 coordination polyhedra in Tables III and IV, respectively.

The substitution of K^+ by Rb^+ selectively expands the a axis and hardly changes the c

[1] F_o–F_c tables and anisotropic thermal parameters are deposited. See NAPS document no. 04405 for 11 pages of supplementary material. Order from NAPS c/o Microfiche Publications, P.O. Box 3513, Grand Central Station, New York, N.Y. 10163. Remit in advance in U.S. funds only $7.75 for photocopies or $4.00 for microfiche. Outside the U.S. and Canada, add postage of $4.50 for the first 20 pages and $1.00 for each of 10 pages of material thereafter, $1.50 for microfiche postage.

TABLE III

METAL–OXYGEN INTERATOMIC DISTANCES AND OXYGEN–OXYGEN EDGE LENGTHS FOR OCTAHEDRAL COORDINATION IN KATO AND RATO

	KATO (Å)	RATO (Å)
M–O_{10}	2.011(1)	2.008(2)
M–O_{11} –O_{12}	1.9540(8)	1.958(1)
M–O_{21} –O_{22}	1.9468(8)	1.944(1)
M–O_{20}	1.905(1)	1.912(2)
Av	1.953	1.954
O_{11}–O_{12} O_{21}–O_{22}	2.9369(1)	2.9375(1)
O_{10}–O_{21} –O_{22}	2.858(1)	2.876(2)
O_{20}–O_{21} –O_{22}	2.831(1)	2.843(2)
O_{20}–O_{11} –O_{12}	2.782(1)	2.782(2)
O_{10}–O_{11} –O_{12}	2.570(2)	2.559(2)
O_{11}–O_{21} O_{12}–O_{22}	2.557(2)	2.549(3)
Av	2.756	2.758

axis, and that of framework cation from Al^{3+} to Mg^{2+} makes 0.9 and 1.2% expansions of the a and c axes, respectively, as can be seen comparing KATO and KMTO

TABLE IV

METAL–OXYGEN INTERATOMIC DISTANCES IN KO_8 AND RbO_8 POLYHEDRA

	KATO (Å)	RATO (Å)
A–O (2a) site	2.978(1) × 8	
A–O (4e) site	2.736(2) × 4 3.307(4) × 4	2.850(1) × 4 3.197(2) × 4

(= $K_{1.54}Mg_{0.77}Ti_{7.23}O_{16}$) (*12*). In Figs. 2a and b, the x and y coordinates of O_{10} and O_{21} atoms are plotted. The figures contain a pair of positions for the compounds except for KATO, i.e., original coordinates and normalized ones by the KATO a axis. Among these original coordinates, the O_{10} atoms in RATO and BATO have relatively large deviations from those in KATO and KMTO. As four oxygen atoms equivalent to O_{10} form a bottleneck window, their movements change a size of the window. In this regard, the normalized positions present more direct information. The window in RATO, KMTO, KATO, and BATO gets smaller in that order and the diagonal length is 5.25, 5.22, 5.18, and 5.10 Å, respectively. In comparison with KATO, the window size in RATO expands by 1.4% in

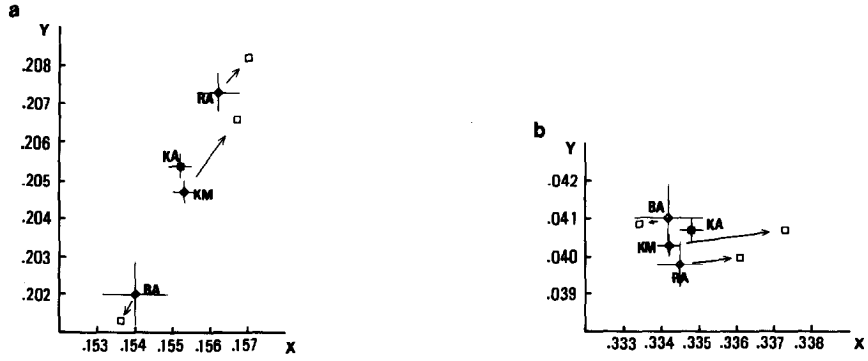

FIG. 2. Variation of oxygen positions with cation substitution. The positions of O_{10} and O_{21} are plotted in (a) and (b), respectively. The marks (◇) designate original coordinates and their normalized ones are indicated by the marks (□). Error bars corresponding to $\pm 3\sigma$ were put on the original coordinates and the same bars on the normalized positions were omitted.

diameter against a 0.5% extension of the *a* axis and that in BATO decreases by 1.7% against a 0.3% axial shrinkage. On the other hand, KMTO gives comparable amounts (1% and 0.9%) of the window and axial expansions. Namely, Rb and Ba make an anisotropic deformation on the frameworks relative to the KATO's, whereas Mg changes the network more uniformly by enlarging octahedra themselves. These suggest a general tendency that the size effects of *A* ions are anisotropic and those of *B* ions are nearly isotropic for the hollandite-type frameworks.

The substitution effects of cations *A* are examined with respect to the geometrical properties of octahedra. The six metal–oxygen bonds in KATO and RATO octahedra are degenerated into four groups as illustrated in Fig. 3a, which is also the case for BATO and KMTO. In the latter, however, reflecting the fact that r_{Mg}(0.72 Å) > r_{Al} (0.54 Å) (*24*), any bonds are enlarged by 0.6 to 1.3% more than the corresponding ones of KATO, and BATO displays specific elongation of the M–$O_{11,12}$ bonds. This elongation is primarily due to the shift of these oxygen atoms toward the Ba^{2+}, which is probably attributable to a doubled charge on the tunnel cation in addition to its

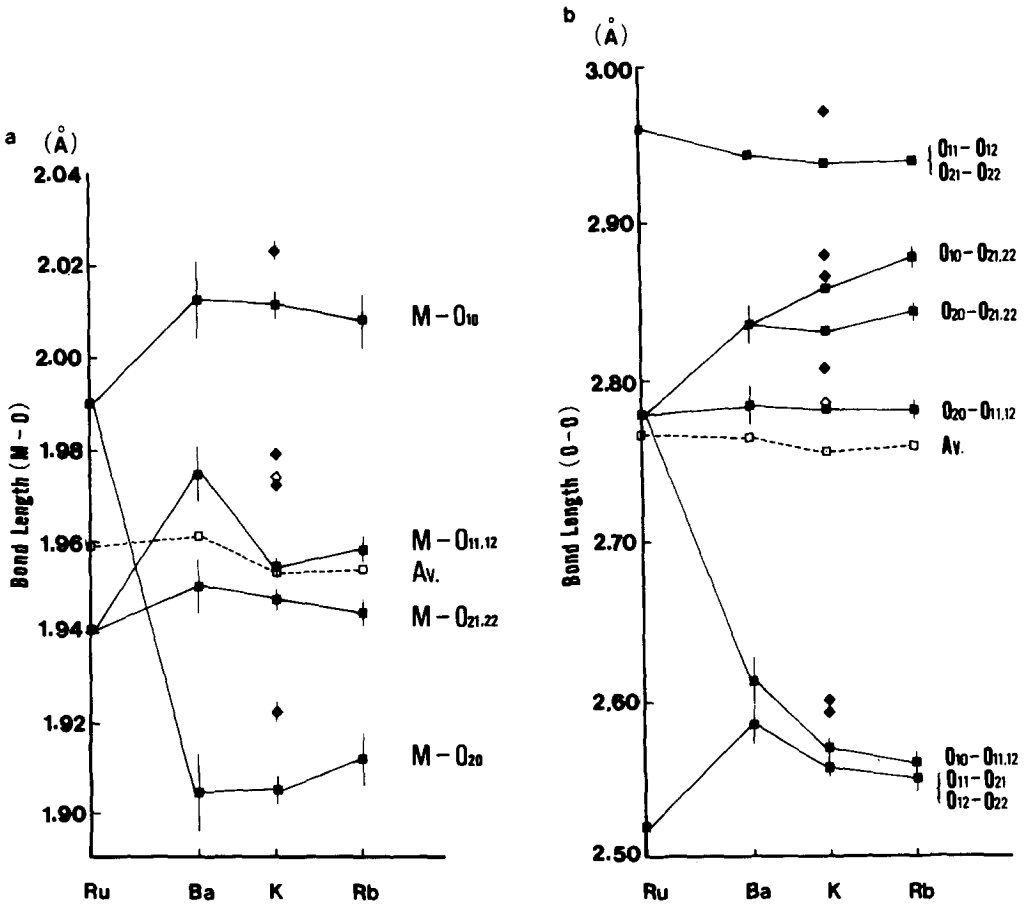

FIG. 3. Comparisons of interatomic distances for metal–oxygen bonds and oxygen–oxygen edges in an octahedron among priderites and rutile. *M*–O bond distances are plotted together with error bars of $\pm 3\sigma$ in (a) and O–O edge lengths in (b). White squares represent the mean bond lengths. Bonds from KMTO are shown by the marks (◆) and (◇). Ba = BATO, K = KATO, Rb = RATO, and Ru = rutile.

smaller radius compared to K^+ and Rb^+. As can be seen in the figure, each priderite gives the distinct separation between the M–O_{10} and M–O_{20} indicating large off-centering of the M atom along the line O_{10}–M–O_{20} in the MO_6 octahedra. Slight separation is also observed between the two middle groups. Exactly, therefore, the central M atoms in the priderites have a three-corner displacement (*25*). Such a displacement does not take place in rutile, whose channel unit (see Fig. 1) is the basic element of a priderite framework.

Twelve oxygen–oxygen edges of the MO_6 octahedron in priderite are degenerated into six groups with two edges each as illustrated in Fig. 3b, but the second and third largest groups in BATO are almost equal in length. It is noteworthy that among the three Al priderites two groups suffer large increases and one large decreases in comparison with the moderate variations of the others with the decreasing radii of the tunnel cations. The reason is again attributed to the displacing O_{10} and its equivalents. In rutile, the shared edges by adjacent octahedra are much shortened as stated in Pauling's rule. It clearly holds in these compounds, too, which have remarkable shortening with shared edges.

In Table V, the octahedron volumes in the priderites and rutile are shown along with the dispersions of O–O and M–O bond lengths; the errors of volumes given correspond to ±3 times standard deviation. The O–O bond dispersion $\Delta_0 = 1/n\Sigma[(R_i - \bar{R})/\bar{R}]^2$ and the M–O bond dispersion $\Delta_M = 1/n\Sigma[(R_i - \bar{R}_i)/\bar{R}_i]^2$, where n is the number of bonds and $\bar{R}$ and $\bar{R}_i$ are a mean length of 12 O–O bonds and a mean M–O distance in each diagonal line O–M–O, respectively. The former factor is considered as representing the degree of distortion from the regular octahedron and the latter as giving a measure of off-center displacement of a central M atom. The comparison of these Al priderites reveals that the Δ_0 reduces and the Δ_M increases with the increasing volume. In other words, the octahedron gets more regular as it becomes larger, but its central cation makes a larger off-center displacement. The increasing regularity from RATO to BATO is based on the fact that certain edges (O_{10}–$O_{11,12}$, O_{11}–O_{21}, O_{12}–O_{22}, and O_{10}–$O_{21,22}$) gradually approach the mean bond length in that order. It implies that the oxygen atoms equivalent to O_{10} are sensitively shifted with the differences in charge and/or size between these tunnel cations. The relation of Δ_0 and V, therefore, may be merely a characteristic of the hollandite-type structure. Similar relations, however, can be expected to take place in other series like RMTO, KMTO, and BMTO.

TABLE V

THE VOLUMES OF OCTAHEDRA IN THE PRIDERITES AND RUTILE AND THE DISPERSIONS OF M–O BOND AND O–O EDGE LENGTHS IN THE OCTAHEDRA

Compound	V (Å^3)	Δ_0 $\times 10^{-3}$	Δ_M $\times 10^{-4}$
RATO	9.71 ± 2	3.01	2.09
KATO	9.74 ± 1	2.72	2.46
BATO	9.88 ± 4	2.14	2.69
KMTO	10.07 ± 1	2.27	2.22
Rutile	9.88	2.15	0

In contrast, the relation between Δ_M and V seems to be more universal. According to Megaw's simple theory (*25*), the off-center displacement of cation M takes place when the cation has the effective size such that the unstressed M–O bond length is less than $1/\sqrt{2}$ times the oxygen effective diameter. In that case, tension occurs along the line O–M–O, and it can be relaxed by the off-centering of cation M. The octahedra in BATO and rutile have the same volume. Assuming that the apparent size of cation M in BATO can be a composition-averaged radius of Ti^{4+} and Al^{3+}, the averaged cation is smaller than Ti^{4+} and hence it can be considered as occupying relatively larger space

than the Ti^{4+} in rutile which has no off-center displacement. The theory suggests a potentiality of the off-centering of the averaged cation in BATO. In fact, an off-center displacement was observed for the compound as shown by the Δ_M. This suggestion is also supported by the tendency for the degree of off-centering in the Al priderites to decrease with decreasing V. Again similar relations may be expected to occur in other series with B cations different from Al^{3+}.

The above relationships simply show what the interaction between the framework and tunnel ions in priderites is like. This seems to be useful for estimating such interactions when ion-conduction phenomena in compounds are studied in further detail.

References

1. J. Bernasconi, H. U. Beyeler, and S. Strässler, *Phys. Rev. Lett.* **42,** 819 (1979).
2. S. Yoshikado, T. Ohachi, I. Taniguchi, Y. Onoda, M. Watanabe, and Y. Fujiki, *Solid State Ionics* **7,** 335 (1982).
3. S. Yoshikado, T. Ohachi, I. Taniguchi, Y. Onoda, M. Watanabe, and Y. Fujiki, *Solid State Ionics* **9** and **10,** 1305 (1983).
4. H. U. Beyeler and S. Strässler, *Phys. Rev. B Condens. Matter* **24,** 2121 (1981).
5. Y. Onoda, Y. Fujiki, S. Yoshikado, T. Ohachi, and I. Taniguchi, *Solid State Ionics* **9** and **10,** 1311 (1983).
6. M. Ishii, Y. Fujiki, and T. Ohsaka, *Solid State Commun.* **55,** 1123 (1985).
7. T. Ohsaka and Y. Fujiki, *Solid State Commun.* **44,** 1325 (1982).
8. H. U. Beyeler, L. Pietronero, and S. Strässler, *Phys. Rev. B Condens. Matter.* **22,** 2988 (1980).
9. A. Byström and A. M. Byström, *Acta Crystallogr.* **3,** 146 (1950).
10. W. Sinclair, G. M. McLaughlin, and A. E. Ringwood, *Acta Crystallogr. Sect. B* **36,** 2913 (1980).
11. J. E. Post, R. B. VonDreele, and P. R. Buseck, *Acta Crystallogr. Sect. B* **38,** 1056 (1982).
12. H-P. Weber and H. Schulz, *Solid State Ionics* **9** and **10,** 1377 (1983).
13. M. C. Cadée and G. C. Verschoor, *Acta Crystallogr. Sect. B* **34,** 3554 (1978).
14. W. Abriel, F. Rau, and K-J. Range, *Mater. Res. Bull.* **14,** 1463 (1979).
15. L. A. Bursill, *Acta Crystallogr. Sect. B* **35,** 530 (1979).
16. Y. Fujiki, T. Sasaki, and M. Kobayashi, *J. Japanese Assoc. Mineral. Petrol. Econ. Geol.* **78,** 109 (1983).
17. H. U. Beyeler, *Phys. Rev. Lett.* **37,** 1557 (1976).
18. M. Watanabe and Y. Fujiki, *J. Solid State Chem.*, **62,** 40 (1986).
19. S. Sasaki, RADY, State Univ. of New York (1982).
20. T. Sakurai, RSSFR-5 in UNICS PROG. SYSTEM (1967).
21. "International Tables for X-Ray Crystallography," Vol. IV, Kynoch Press, Birmingham. (1974).
22. M. Tokonami, *Acta Crystallogr.* **19,** 486 (1965).
23. S. Sasaki, KEK-Report (National Laboratory for High Energy Physics in Japan), 83-22 (1984).
24. R. D. Shannon, *Acta Crystallogr. Sect. A* **32,** 751 (1976).
25. H. D. Megaw, *Acta Crystallogr. Sect. B* **24,** 149 (1968).